2021

Investigating the AGN-Merger Connection Using Close Galaxy Pairs in the CANDELS Fields

Sean L. Dougherty
Colby College

Investigating the AGN-Merger Connection Using Close Galaxy Pairs in the CANDELS Fields

Sean Dougherty[1] and Dale Kocevski[1]

[1]*Department of Physics and Astronomy,*

Colby College, Waterville, Maine 04901, USA

(Dated: May 22, 2021)

Abstract

Galaxy mergers are catastrophic events in that they greatly change the properties of the galaxies involved. Observations of the nearby universe suggest that they may also be able to trigger active galactic nuclei (AGN) even prior to the final coalescence, though there is much controversy surrounding this belief, particularly at high redshifts. In order to address this question, we have assembled a large sample of photometric galaxy pairs within the GDS and EGS fields of the CANDELS survey. We use photometric redshift probability distribution functions and the combined redshift probability function to assign probabilities for each projected pair. We incorporate pair probabilities into a survey of X-ray detected AGN to calculate weighted AGN fractions and AGN enhancements for interacting galaxies. Overall, for both major and minor mergers at $0.5 < z < 3.0$, we find that AGN frequency is enhanced by 1.30 ± 0.17, 1.54 ± 0.24, and 3.21 ± 0.72 in pairs separated by $20 < d < 30$, $10 < d < 20$, and $d < 10$ kpc respectively. We also separately investigate AGN enhancement in minor and major mergers and find that minor mergers might play a larger role than major mergers in triggering AGN at high redshifts. Finally, we investigate how redshift affects AGN enhancement in pairs, and we find no enhancement in galaxies at $1.5 < z < 3.0$. However, more complete AGN surveys at high redshifts are required to confirm this trend.

Acknowledgements **3**

1. Introduction **4**

2. Data **8**

3. Sample Selection **10**

3.1 Sample Cleaning 11

3.2 Selection Criteria 11

3.3 The Pair Probability Function 12

3.4 Counting Fractional Pairs 13

3.5 Control Samples 15

3.6 Analysis of AGN Activity 15

4. Results **16**

5. Discussion **21**

5.1 The AGN-Merger Connection 21

5.2 Caveat and Future Work 28

6. Summary **29**

7. References **30**

Appendix I: Detailed AGN Enhancement Data **37**

ACKNOWLEDGEMENTS

First, I'd like to thank my advisor, Prof. Dale Kocevski for his continual help and guidance during this process. Coming into this year, I was unsure whether I would be able to complete a thesis project given the extraordinary circumstances. I am greatly indebted to Prof. Kocevski for giving me the opportunity to pursue such rewarding research during this hectic time. Today, I am proud to say that I completed my thesis entirely remotely. I'd also like to thank the Department of Physics and Astronomy for constantly challenging me and encouraging me to always ask questions.

Finally, I'd like to thank my friends and family for their endless support not only during this project but also over the past four years. This thesis is dedicated to my grandfather ("Grandpa"), who always inspired me with his diligence and kindness.

1. INTRODUCTION

Over the past two decades, observational studies have demonstrated a close correlation between the mass of a galaxy's stellar bulge and its supermassive black hole (SMBH), which relationship suggests that a galaxy and its SMBH evolve simultaneously (Magorrian et al. 1998; Gebhardt et al. 2000; Tremaine et al. 2002; Gültekin et al. 2009; McConnell & Ma 2013). Galaxy mergers/interactions are known to have significant impacts on galaxy properties, such as star formation rate (SFR; Ellison et al. 2008, 2013b; Patton et al. 2013) and galaxy morphology (Lotz et al. 2008; Darg et al. 2010; Ellison et al. 2010). Likewise, if active galactic nuclei (AGN) activity is also triggered by galaxy interactions, then this could help explain an important stage in the co-evolution of galaxies and their SMHBs.

Simulations of gas-heavy galaxy mergers in the local universe predict that merging events could provide the torque necessary to reduce angular momentum and trigger gaseous inflows into the SMBH (Barnes & Hernquist 1991; Mihos & Hernquist 1996; Di Matteo et al. 2008; Hopkins et al. 2009). Additionally, numerous studies have demonstrated that merging galaxies enhance SFRs (Kennicutt et al. 1987; Barton et al. 2000; Lambas et al. 2003; Alonso et al. 2004; Nikolic et al. 2004; Woods & Geller 2007; Ellison et al. 2008, 2010; Liu et al. 2011; Patton et al. 2011) and signs of gas inflows as evidenced by diluted interstellar medium metallicities (Kewley et al. 2006; Ellison et al. 2008; Michel-Dansac et al. 2008; Kewley et al. 2010; Rupke et al. 2010; Scudder et al. 2012). Nonetheless, many other processes are capable of triggering AGN feuling, such as a secular loss of angular momentum in the bar or spiral arms, steady-state accretion of diffuse hot gas, or interactions with nearby star clusters or gas clouds. Still, there is much debate over the role, if there is one, galaxy mergers play in triggering AGN.

Attempts to characterize the AGN-merger connection have produced mixed results. Using a sample of low-redshift ($0.01 < z < 0.20$) galaxies undergoing a minor or major merger (mass ratio < 10) from the Sloan Digital Sky Survey (SDSS), Ellison et al. (2011) find a clear increase in AGN enhancement at decreasing projected separations (< 40 kpc) compared to a mass- and redshift-matched control sample of isolated galaxies. They classify galaxies as AGN based on ratios of strong emission lines or spectral identification as quasi-stellar objects. At the smallest projected separations of interacting galaxies (< 10 kpc), they determine that AGN enhancement increases by a factor of ~ 2.5. Various other observations of the

nearby universe with comparable selection criteria and methodology find similar results (Alonso et al. 2007; Woods & Geller 2007; Ellison et al. 2013a, 2019; Satyapal et al. 2014; Weston et al. 2017). In contrast, using a sample of high-redshift ($0.5 < z < 3.0$) major spectroscopic galaxy pairs (mass ratio < 4) from the COSMOS and CANDELS fields, Shah et al. (2020) find no significant AGN enhancement at decreasing separations compared to a mass-, redshift-, and environment-matched control sample of isolated galaxies. They classify galaxies as AGN based on X-ray luminosity thresholds and IR broadband colors. At the smallest projected separations of interacting galaxies (< 25 kpc), they compute AGN enhancements of 0.94 and 1.00 for X-ray and IR-selected AGN respectively. While there are not many studies done on this at high redshifts, a number of them have also not found any AGN-merger connection out to $z \sim 1$ (Grogin et al. 2005; Pierce et al. 2007; Cisternas et al. 2011; Kocevski et al. 2012; Schawinski et al. 2012).

One possible explanation for the discrepancies among these results is their sample selection criteria, as AGN depend substantially on various galaxy properties such as mass, luminosity, color, and gas concentration. In particular, differences in mass and redshift between studies could be responsible for the conflicting results. Ellison et al. (2011) notes that in merging galaxies, there is a clear trend of increasing galaxy mass at decreasing physical separations. Since there is a strong correlation between AGN activity and galaxy mass, the increase in galaxy mass at low separations could artificially inflate AGN enhancement. Furthermore, galaxy mass tends to be higher at lower redshifts, so interacting galaxies in the nearby universe are more likely to exhibit relatively large AGN fractions. Additionally, not only do massive spiral galaxies have much higher gas fractions ($\sim 50\%$) at $z \sim 2$ than at $z \sim 0$ ($\sim 10\%$) (Daddi et al. 2010; Tacconi et al. 2010; Scoville et al. 2014), but high-redshift galaxies also have a much clumpier gas distribution (Stott et al. 2016). Even though an abundance of gas could more easily be funneled into the central SMBH during a galaxy interaction, the high turbulence and velocity dispersion caused by areas with high gas concentrations could limit the inflows of gas into the SMBH. Alternatively, hydrodynamic instabilities in highly gaseous regions could trigger gas inflows without the need for a merging event. Using data from the CANDELS survey, Kocevski et al. (2012) show that $\sim 50\%$ of X-ray-selected, moderate-luminosity ($L_x < 10^{43}$ erg s^{-1}) AGN at $z \sim 2$ are more likely to be triggered stochastically by secular processes and/or disk instabilities than a merger. Morphological studies have produced mixed results in determining what portion of AGN

populations appear to be caused by mergers, as Donley et al. (2018) show that IR-selected, high-luminosity AGN at $z \sim 2$ are much more likely ($\sim 75\%$ versus $\sim 31\%$) to be classified as merging compared to X-ray-selected AGN at the same redshift. Still, simulations and observations support that AGN enhancement increases at lower redshifts and that galaxy interaction is increasingly important in triggering SMBH activity as the universe evolves (Di Matteo et al. 2008; Fensch et al. 2017; McAlpine et al. 2020).

Inconsistencies among results could also be due to the various methods studies use to identify AGN. For the most part, AGN are detected with strong emission line flux ratios, spectral classifications, X-ray luminosity thresholds, or IR broadband colors. Each of these methods, however, identify different components of an AGN, such as the dusty torus, accretion disk, ratio lobes, emission line regions, or jets. AGN surveys done using strong emission line flux ratios and spectral classification are unreliable at high redshifts due to the small and faint nature of those galaxies. Selecting AGN based on X-ray emission is somewhat reliable at high redshifts, as only an AGN will emit intense X-ray radiation in a galaxy. However, the extreme column densities ($N_H > 10^{24}$ cm^{-2}) of Compton-thick AGN are capable of absorbing hard X-ray photons (Comastri et al. 1995; Ueda et al. 2003; Gilli et al. 2007; Akylas et al. 2012). Likewise, analyses of the diffuse X-ray background reveal that Compton-thick obscuration hides upto half of all AGN (Comastri et al. 1995; Ueda et al. 2003; Gilli et al. 2007; Akylas et al. 2012). In a study of host morphologies of heavily obscured AGN at $z \sim 1$, Kocevski et al. (2015) suggest that Compton-thick AGN represent a distinct phase in SMBH growth and galaxy evolution resulting from a merging/interacting event. Identifying AGN based on re-emitted IR radiation from obscuring circumnuclear dust is a potential bypass to this X-ray caveat (Lacy et al. 2004; Stern et al. 2005; Daddi et al. 2007; Donley et al. 2007; Soifer et al. 2008); however, morphological studies of IR-selected AGN have produced inconsistent findings on the disturbed nature of obscured AGN versus unobscured AGN (Schawinski et al. 2012). Since regions of intense star formation can also produce IR radiation, IR surveys tend to be skewed towards high luminosity AGN (Draper & Ballantyne 2012; Treister et al. 2012). Consequently, it's possible that different AGN selection methods could produce biased AGN enhancement results based on whether interacting AGN are more likely to be better detected by either IR or X-ray surveys.

Most previous methods of identifying AGN in interacting galaxies depend on the AGN and merger being detectable simultaneously. However, some studies suggest that there is

a delay between when a merging event triggers an AGN and when that AGN is detectable (Storchi-Bergmann et al. 2001; Schawinski et al. 2009; Cisternas et al. 2011; Mendez et al. 2011). Models almost always predict that gas inflow rates and the corresponding AGN duty cycle culminate during post-merger phases, where the stellar bulge appears undisturbed (Di Matteo et al. 2005; Li et al. 2008; Johansson et al. 2009; Hopkins & Quataert 2010; Hopkins 2011; Snyder et al. 2011; Hopkins et al. 2012; Ellison et al. 2013a). While mergers can prompt gas inflows into a SMBH, the resulting accretion may not be intense enough to produce detectable AGN signatures until later in the merging process. In this sense, it is difficult not only to accurately survey disturbed AGN but also to determine the separation between the merging galaxies where AGN triggering begins.

Another major disparity in works mentioned above has to do with the different methods of classifying galaxy mergers. In general, mergers are identified based on either morphological signs of disturbances, such as tidal bridges, double nuclei, or tidal tails, or with close projected companions. These methods are mutually exclusive, however, and, just as in AGN identification, surveys probe different aspects and timescales of galaxy mergers based on their selection methodology. While studying morphological disturbances and identifying projected pairs are effective methods at surveying complementary properties of mergers, both methods become much more challenging at high redshifts. Due to the low surface brightness of high-redshift galaxies, it is difficult to distinguish reliably observable merging signatures (Lotz et al. 2008; Younger et al. 2009; Puech et al. 2012; Snyder et al. 2013). For similar reasons, the redshifts needed to determine projected pairs take on large uncertainties.

In finding galaxy companions, studies primarily use spectroscopic or photometric redshifts. While spectroscopic redshift surveys have little uncertainty in the near universe, they become more sparse at higher redshifts. Spectroscopic redshifts can only be determined if an unobscured galaxy exceeds a mass and flux threshold, and for studies of the most massive merging galaxies ($\log_{10}(M_*/M_\odot) > 11$) at $z > 1$, spectroscopic surveys are often complete (Bluck et al. 2009; Man et al. 2011). However, at higher redshifts, the amount of these galaxies decreases to a point where there may not be a statistically significant amount of merging galaxies detectable through spectroscopic surveys in the CANDELS fields (Ilbert et al. 2013; Muzzin et al. 2013; Mortlock et al. 2014; Duncan et al. 2014). Additionally, spectroscopic redshift surveys are more likely to miss galaxies either disturbed by a merging event or obscured by an AGN, particularly at high redshifts. Consequently, using

spectroscopic redshifts to identify close pairs in a study of AGN enhancement as a function of projected separation may be problematic.

Despite the high uncertainties (best scatters range from 0.01 to 0.04; Molino et al. 2014), photometric redshifts could provide a more complete analysis of merging galaxies at high redshifts. Distinguishing true galaxy pairs from line-of-sight projected pairs is the greatest limitation of photometric redshift surveys. Previous attempts to correct for this constraint, such as using de-projected two-point correlation functions (Bell et al. 2006; Robaina et al. 2010), correcting for chance pairs by searching over random positions in the sky (Kartaltepe et al. 2007), and integrating the mass or luminosity function around the target galaxy to estimate the number of random companions (Le Févre et al. 2000; Bluck et al. 2009; Bundy et al. 2009), have been unable to incorporate photometric redshift uncertainties into derived properties, such as stellar mass or rest-frame magnitude. This absence could potentially result in inconsistent mass or luminosity sample selections. Instead, using photometric redshift probability distribution functions (PDFs) and a probabilistic pair count methodology, as outlined by López-Sanjuan et al. (2015) and developed by Duncan et al. (2019), has been shown to produce accurate merger fractions in high-redshift galaxies without spectroscopic redshifts.

The structure of this paper is as follows. We describe the survey data and photometric redshift PDFs used in Section 2. In Section 3, we discuss our pair and control galaxy sample selection. We present our results in Section 4, and we elaborate on their implications for the AGN-merger connection in section 5.1. In section 5.2, we describe some of the limitations of our study and how they could be improved upon in future works. Section 6 summarizes our findings.

2. DATA

Our parent sample of massive galaxies is drawn from HST/WFC3 F160W (H-band) selected catalogs in four of the five CANDELS fields (Grogin et al. 2011; Koekemoer et al. 2011). This includes the Great Observatories Origins Deep Survey (GOODS; Giavalisco et al. 2004) north and south fields, the UKIDSS Ultra Deep Survey (UDS; Cirasuolo et al. 2007; Lawrence et al. 2007), and the Extended Groth Strip (EGS, Davis et al. 2007). Point-source depths vary among the CANDELS fields from $H = 27$ in the wide fields to

$H = 27.7$ in the deep fields (see Grogin et al. 2011). Multiwavelength photometry (U-band to 8 m) was measured in each field using the TFIT routine (Laidler et al. 2006) as described in detail in Guo et al. (2013), Galametz et al. (2013), Stefanon et al. (2017), and Barro et al. (2017) for the GOODS-S, UDS, EGS, and GOODS-N fields, respectively. Photometric redshifts were computed in each field using the method described in Dahlen et al. (2013) and resulted in typical errors of $\Delta z(1+z) = 3\%$ at $z > 1.5$. Stellar masses were computed as described in Mobasher et al. (2015) and Santini et al. (2015). Rest-frame photometry was derived by fitting templates to the observed-frame spectral energy distributions (SEDs) using the EAZY code (Brammer et al. 2008), as described in Kocevski et al. (2017). Visual extinction values, A_V, were derived using FAST (Kriek et al. 2009) assuming a Chabrier (2003) initial mass function, solar metallicity, exponentially declining star formation histories, and the Calzetti et al. (2000) dust extinction law (see Wuyts et al. 2011 for additional details). Galaxy morphologies and sizes were measured from the HST/WFC3 H-band images using GALFIT (Peng et al. 2002) as described in van der Wel et al. (2014). This includes Sérsic indicies and effective (half-light) radii.

X-ray detections in all fields except the UDS come from publicly available Chandra point-source catalogs. In GOODS-south and north, we make use of the 4 Ms and 2 Ms point-source catalogs of Xue et al. (2011) and Xue et al. (2016), respectively, while for EGS, we use the 800 ks source catalog presented in Nandra et al. (2015). In UDS, we use a source catalog from the X-UDS survey (PI. G. Hasinger; Kocevski et al. 2017). These observations consist of 25 Chandra/ACIS-I pointings mosaiced to achieve $\sim$ 600 ks depth in the area of UDS imaged by CANDELS.

To identify merging galaxies that host AGN, optical counterparts to X-ray sources in each field except the UDS were taken from the literature. In GOODS-N and GOODS-S, we adopt the H-band counterparts provided in Xue et al. (2016) and Hsu et al. (2014), while in EGS we use the counterparts identified in Nandra et al. (2015). In the UDS, we matched the X-UDS source catalog to the CANDELS H-band catalog of Galametz et al. (2013) using the maximum likelihood technique described in Sutherland & Saunders (1992) and more recently implemented by Civano et al. (2012). In short, the method gauges the likelihood that a H-band source is matched to an X-ray source by comparing the probability of finding a genuine counterpart with the positional offset and magnitude of the optical candidate relative to that of finding a similar object by chance. Likelihood ratios were calculated for

all galaxies within 5" of an X-ray source, taking into account the positional uncertainty of the X-ray centroid and the magnitude of the possible counterpart galaxy. A likelihood threshold is set that maximizes both the completeness and reliability of the crossmatches (see Civano et al. 2012 for details), and optical matches with likelihood ratios above this threshold are deemed secure.

In each field, X-ray luminosities in the soft (0.5–2 keV), hard (2–8 keV) and full (0.5–8 keV) bands are then computed from the observed fluxes in each band using the best available CANDELS redshift (which are a combination of ground-based spectroscopic and photometric redshifts) and K-corrected assuming a power-law spectrum with a spectral slope of $\Gamma = 1.4$. Sources with X-ray luminosities in excess of 10^{42} erg s^{-1} in any band are then flagged as AGN since the X-ray emission from high-mass X-ray binaries in star-forming galaxies rarely exceeds this luminosity (Alexander et al. 2005).

The photometric redshift probability distribution functions (PDFs) used in this analysis are a combination of six PDFs determined independently within the CANDELS collaboration. All PDFs were determined using code that fits a set of SED templates to a galaxy based on possible redshift, from which they calculate χ^2. The codes used were EAZY (used by two groups; Brammer et al. 2008), zphot (Giallongo et al. 1998; Fontana et al. 2000), HyperZ (Bolzonella et al. 2000), LePhare (Arnouts & Ilbert 2011), and WikZ (Wiklind et al. 2008). Using a Q-Q plot, Kodra (2019) determined the optimal shift and exponentiation parameters of each PDF, and they combined them using a Hierarchical Bayesian (HB) methodology analogous to that in Dahlen et al. (2013). They also combined them using the minimum Fréchet Distance, but their HB result yielded the smallest average normalized median absolute deviation (0.022) and average outlier rate (4.6%).

3. SAMPLE SELECTION

In order to account for all potential merging/interacting galaxies, we use a neighbor excess methodology. Numerical simulations suggest that most galaxies will eventually merge if their dark matter halos are within a certain separation distance (Kitzbichler & While 2008); though, that specific distance is often debated. While Duncan et al. (2019), who also utilize photometric redshift PDFs, define the merging projected separation on the plane of the sky, d, as $d < 20$ to 50 kpc, most surveys consider the maximum interacting separation to be

$d < 80$ to 100 kpc (Patton et al. 2011; Scudder et al. 2012; Ellison et al. 2013b). Likewise, we consider a galaxy pair with $d < 80$ kpc to be merging/interacting.

In this study, we first identify projected galaxy pairs through an angular separation analysis. We make cuts to our sample based on galaxy and merger properties, such as redshift, stellar mass, and stellar mass ratio. Then, using the photometric PDFs and the pair probability function, we determine the probability a galaxy is merging with another galaxy at the same redshift, and we assign that probability as a weight in our AGN enhancement analysis. As shown in López-Sanjuan et al. (2015), the use of photometric redshift PDFs to identify true physical galaxy pairs is an effective way to account for redshift and relative velocity difference uncertainties as well as line-of-sight projected pairs, which would otherwise need to be subtracted from pair counts using complex statistical techniques, such as with a Monte Carlo simulation.

3.1 Sample Cleaning

Before making initial galaxy selections within the photometric catalog, we must first clean the data for unreliable galaxy entries, such as those with a high likelihood of being a star or image artefact. To account for stellar objects, we exclude all sources with a stellar class greater than 0.9. In order to account for erroneous SED fits caused by photometries contaminated by image artefacts, such as diffraction spikes or edge effects, we only select galaxies without flags in the photometry flag map (see e.g. Guo et al. 2013; Galametz et al. 2013). Finally, to make sure we select galaxies with workable data, we exclude sources with photometric redshift PDFs that either don't resemble a Gaussian distribution (e.g. more than one peak or no distinct peak) or have a $1\sigma > 0.30$ around the peak redshift estimate.

3.2 Selection Criteria

Aside from the aforementioned cleaning cuts, we use the following criteria to generate a preliminary sample of galaxy pairs that are either interacting or have interacted in the past:

1. *Redshift:* The best redshift estimate, whether photometric or spectroscopic, must be between 0.5 and 3.0.

2. *Mass Limit:* The stellar mass of each galaxy must be greater than 10^9 $M_\odot$.

3. *Stellar Mass Ratio:* The stellar mass ratio of merging galaxies must be greater than 1:10. Typically, a ratio greater than 1:4 denotes a major merger and a ratio greater than 1:10 but less than 1:4 denotes a minor merger.

4. *Projected Separation:* The projected separation between pairs must be less than 80 kpc.

Using the coordinates and best redshift estimate of each galaxy, we create an initial sample of projected galaxy pairs based on a minimum and maximum angular separation. With a given redshift and cosmology, the angular separation between two galaxies, $\theta(z)$, is

$$\theta(z) = \frac{d}{d_A(z)}, \tag{1}$$

where d is the projected distance and $d_A(z)$ is the angular diameter distance. For each galaxy, this metric tells us which objects on the plane of the sky would be within the 80 kpc projected separation distance if they were at the same redshift. For convenience, we consider the galaxy whose best redshift estimate is used in the angular separation distance calculation as the 'prime' galaxy and all others that fall within its separation limits as 'partner' galaxies. Since many galaxies have high uncertainties associated with their best redshift estimates and the angular separation cut depends on the redshift of only the prime galaxy, we consistently define the prime galaxy in a pair as the more massive galaxy. This way we avoid the possibility of the same pair being sorted into multiple projected separation bins, one calculated based on the best redshift estimate of the more massive galaxy and one on that of the less massive galaxy. While there are some pairs missed using this methodology (e.g. the partner galaxy does not fall within the maximum angular separation of the prime galaxy but the prime galaxy does fall into the maximum angular separation of the partner), these count for an insignificant percentage of the total sample, especially at the larger projected separation bins.

3.3 The Pair Probability Function

For a given projected pair of galaxies, the combined redshift probability function, $Z(z)$, is defined as

$$Z(z) = \frac{2 \times P_1(z) \times P_2(z)}{P_1(z) + P_2(z)}, \tag{2}$$

where $P_1(z)$ and $P_2(z)$ are the photometric redshift PDFs of the prime and partner galaxies respectively. Likewise, the probability the two galaxies in question are a true physical pair, w, is given by

$$w = \int_0^\infty Z(z)dz. \tag{3}$$

Once we have a preliminary catalog of projected pairs, we find the pair weight, w, associated with each pair and assign that value to both the prime and partner galaxies as the probability that that galaxy has a true physical pair. For example, Figure 1 shows three separate applications of the pair probability function within the GOODS South field of the CANDELS survey. While each pair satisfies the base selection criteria and angular separation limits, they have varying pair probabilities. Additionally, the advantage of this methodology is that it is capable of working with photometric redshifts with high uncertainties, which are incorporated into this pair probability statistic.

3.4 Counting Fractional Pairs

At this point, the galaxy pairs, along with their pair weights, are sorted into eight bins of different projected separation distances ranging from 0 to 80 kpc. We account for duplicates in the event that the same galaxy has more than one pair in a single bin. In contrast to Duncan et al (2019), who focus on pair fractions, we focus on AGN fractions, which requires only the identification of individual galaxies that have experienced an interaction. In other words, the properties of the partner galaxy in an AGN enhancement analysis is unimportant in the study beyond the aforementioned criteria.

There are significantly less interacting galaxies with $d < 10$ kpc, as the ability to distinguish two galaxies at such a small separation and high redshift is difficult due to the limitations of SED fitting. Nonetheless, our methodology accurately identifies mergers at projected separations down to 5 kpc. Below separations of 5 kpc, selected galaxy pairs require visual confirmation, as pairs at smaller projected separations are more likely to exhibit visual interaction signatures and less likely to be line-of-sight projections (Shah et al. 2020). However, visual identification, as previously mentioned, is not a comprehensive method of merger identification at high redshift because it strongly depends on properties of the merging galaxies such as gas fractions, morphological types, and orbital parameters. While we are limited by our ability to thoroughly identify mergers at small projected separations, we

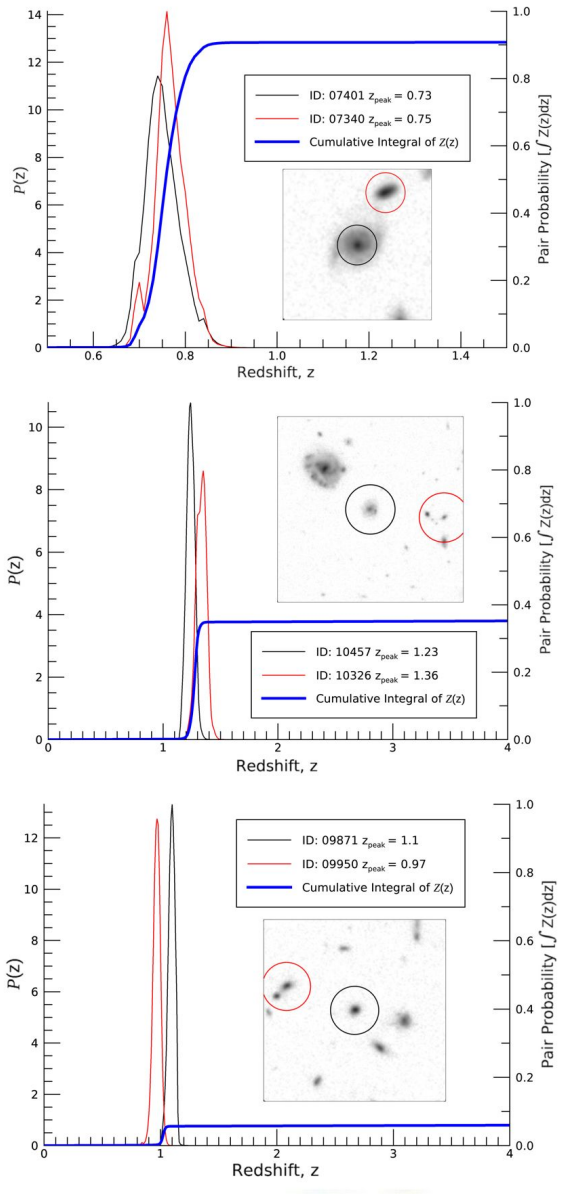

FIG. 1. Example photometric redshift PDFs and integrated pair probability functions, $Z(z)$, for projected galaxy pairs within GDS. In each panel, the black line corresponds to the PDF of the prime galaxy and the red line corresponds to that of a projected partner galaxy. The blue line represents the cumulative integral of $Z(z)$ for the pair. The cutouts show the H_{160} image of the pair centered on the prime galaxy. Just as before, the black circle surrounds the primary galaxy while the red circle surrounds the projected partner galaxy.

are still able to collect a sample of 365 galaxies with $d < 10$ kpc bin, 17 of which have a pair probability greater than 0.1.

Since every projected pair has a nonzero pair probability, we do not apply a probability threshold for merging galaxies in our sample. Instead, we are interested in fractional galaxies with a true physical pair. In this sense, a group of galaxies with pair probabilities 0.21, 0.98, 0.01, 0.56, and 0.02 will have 1.78 true pairs. In the scenario a prime galaxy has more than one companion in one bin, the prime galaxy receives the highest pair probability of all its matches. In the following AGN enhancement analysis, these pair probabilities will be used as weights in determining the total number of fractional AGN in a sample.

3.5 Control Samples

In order to best study the effects of interacting galaxies on AGN activity, we assemble a control sample of mass- and redshift-matched isolated galaxies. As discussed before, AGN activity has a strong correlation with mass and redshift; likewise, it is important that these factors are matched in the control sample. Some studies of AGN enhancement as a function of projected separation environmentally match their control sample with the parent sample (e.g. Shah et al. 2020), but matching local galaxy densities for both interacting galaxies and isolated galaxies is contradictory. By including environmentally matched control galaxies, we would be accounting for the effects of nearby sources on our control sample. Recall that we are most interested in studying SMBHs in interacting environments versus isolated environments, so including an environment-matched control sample might yield artificially inflated AGN enhancements. Consequently, for every interacting galaxy, we iteratively select two galaxies of similar mass and redshift with no close projected companion within 80 kpc. If there is not more than one isolated galaxy with redshift and mass within $\pm$ 0.2 and $\pm$ $\log_{10}(2)$ $M_{\odot}$ respectively of the corresponding merging galaxy, then only one control galaxy is selected. Additionally, we require that all control galaxies satisfy the initial criteria outlined in the Sample Cleaning section, and we select control galaxies from the same field as the analogous parent samples.

3.6 Analysis of AGN Activity

In each bin, we have assembled a list of potentially interacting galaxies, each with their own probability of having a true companion. To examine the AGN enhancement of our

sample versus the control sample, we calculate the weighted AGN fraction, F_{AGN}, for each bin using

$$\text{Weighted AGN Fraction} = F_{AGN} = \frac{\sum_j w_j \times M^{\text{AGN}_j}}{\sum_j j}, \tag{4}$$

where M^{AGN}, whether a galaxy hosts an AGN or not, is

$$M^{\text{AGN}} = \begin{cases} 1, & \text{if AGN} \\ 0, & \text{if no AGN.} \end{cases} \tag{5}$$

The pair probability, w, now acts as a weight in determining fractional AGNs in each galaxy. Similar to how we calculated fractional galaxies with a true pair above, we are interested in finding the total fractional AGN in our sample. Considering the average AGN weight is 0.19, our weighted AGN fractions are considerably less than those of similar studies.

To determine the weighted AGN fraction of the control sample, we first calculate the unweighted AGN fraction of each control bin then multiply those values by the average AGN weight of the entire parent sample (all bins included) for each corresponding field. This way, selected control AGN are weighted consistently with their parent sample.

In each bin, we define the AGN enhancement as the ratio of the weighted AGN fraction of interacting galaxies to that of the isolated control galaxies:

$$\text{AGN Enhancement} = \frac{\text{Weighted AGN Fraction}_{\text{Pairs}}}{\text{Weighted AGN Fraction}_{\text{Controls}}}. \tag{6}$$

Assuming binomial statistics, we calculate the 1σ error (Cameron 2011) for each bin of interacting galaxies with

$$\sigma = \sqrt{\frac{\bar{w} \times F_{AGN}(1 - F_{AGN})}{n}}, \tag{7}$$

where $\bar{w}$ is the average pair weight in each bin, and n is the size of the sample. For the control sample, the 1σ error is calculated the same way, except $\bar{w}$ is the average pair weight for that field and F_{AGN} corresponds to the control galaxy weighted AGN fractions.

With this methodology, we investigate AGN enhancement in merging/interacting galaxies while varying initial selection criteria, such as redshift, mass limit, and stellar mass ratio.

4. RESULTS

Weighted AGN fraction as a function of projected separation for major mergers in EGS and GDS is shown in Figure 2, and AGN enhancement as a function of projected separation

for this scenario is shown in Figure 3. While there is significant AGN enhancement in pairs separated by less than 10 kpc (3.63 $\pm$ 0.88), there is only very slight enhancement out to 30 kpc (1.08 $\pm$ 0.21 in $10 < d < 20$ kpc and 1.23 $\pm$ 0.19 in $20 < d < 30$ kpc). Of all mergers in this survey, 70.7% are classified as major mergers. Likewise, when we include minor mergers in this survey, we get a more complete picture of the role mergers play in triggering AGN.

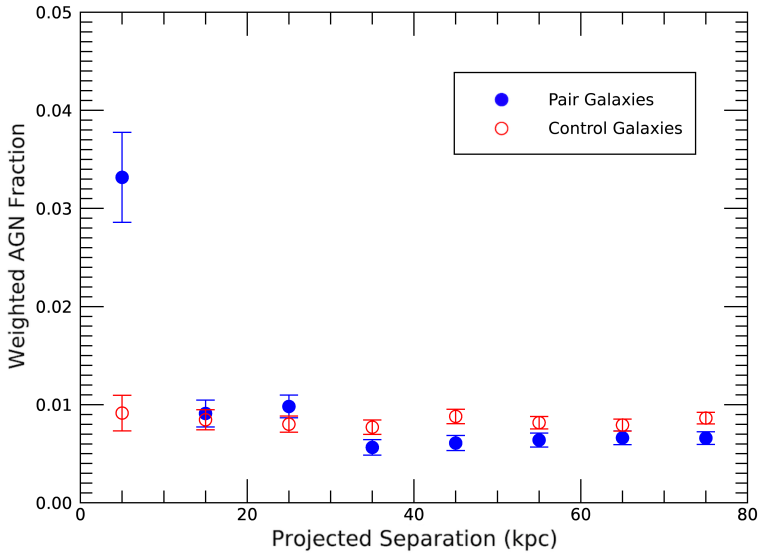

FIG. 2. Weighted AGN fraction as a function of pair separation for galaxies undergoing a major merger at $0.5 < z < 3.0$ in GDS and EGS. Galaxies with a projected pair are indicated by blue filled circles. Mass- and redshift-matched isolated galaxies are indicated by open red circles. The error bars correspond to 1σ binomial confidence intervals.

Weighted AGN fraction as a function of projected separation for all mergers in EGS and GDS is shown in Figure 4, and detailed results are presented in Table 1 of Appendix I. AGN enhancement as a function of projected separation in these galaxies is shown in Figure 5. In these galaxies, there is a clear trend of increasing AGN enhancement at decreasing projected separation beginning at 30 kpc. The $20 < d < 30$, $10 < d < 20$, and $d < 10$ kpc bins show AGN enhancements of 1.30 $\pm$ 0.17, 1.54 $\pm$ 0.24, and 3.21 $\pm$ 0.72 respectively. Galaxies separated by more than 30 kpc have enhancements similar to isolated galaxies, and their combined weighted AGN fraction is 0.76 $\pm$ 0.03% where that for all isolated galaxies is 0.90 $\pm$ 0.02%. A substantial amount of mergers in this survey are minor mergers, and these must be responsible for increasing AGN enhancements in our whole sample.

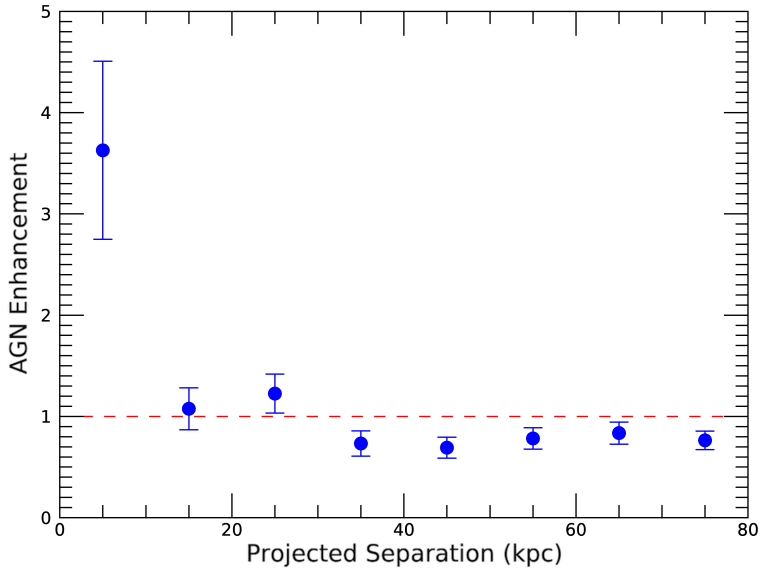

FIG. 3. The level of AGN enhancement as a function of pair separation for galaxies undergoing a major merger at $0.5 < z < 3.0$ in GDS and EGS. The error bars correspond to appropriate propagation of 1 binomial confidence intervals. The dashed red line reflects an AGN enhancement of 1, where the weighted AGN fractions for control galaxies would exactly equal that for isolated galaxies.

Weighted AGN fraction as a function of projected separation for minor mergers in EGS and GDS is shown in Figure 6, and AGN enhancement as a function of projected separation for this scenario is shown in Figure 7. Minor mergers exhibit AGN enhancement out to projected separations less than 40 kpc. Galaxies separated by $30 < d < 40$, $20 < d < 30$, and $10 < d < 20$ kpc demonstrate increasing AGN enhancements of 1.26 ± 0.25, 1.71 ± 0.38, and 2.78 ± 0.66 respectively. However, AGN enhancement for minor mergers peaks at $10 < d < 20$ kpc, and minor mergers with d < 10 kpc show AGN enhancement of only 2.08 ± 1.17. This could be due to the difficulty of distinguishing two galaxies of different sizes and luminosities at such small separations. If we focus our study on just minor mergers, we see not only generally higher AGN enhancements but also AGN enhancements at farther projected pair separations.

Since our methodology allows us to resolve merging galaxies at high redshifts, we can isolate redshift ranges in our initial sample selection criteria to examine how redshift affects AGN enhancement. Since the median redshift in our full sample is $\tilde{1}.50$, we sort our sample into two redshift bins: $0.5 < z < 1.5$ and $1.5 < z < 3.0$. Weighted AGN fraction as a function

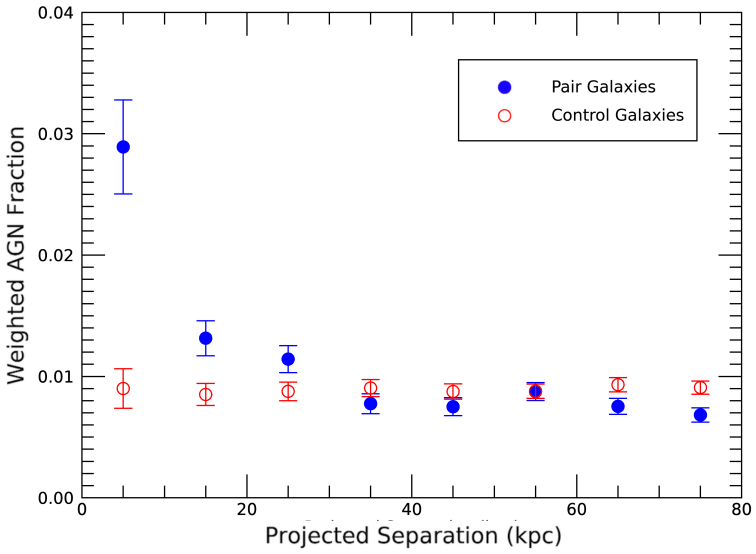

FIG. 4. Weighted AGN fraction as a function of pair separation for all merging galaxies at $0.5 < z < 3.0$ in GDS and EGS. Galaxies with a projected pair are indicated by blue filled circles. Mass- and redshift-matched isolated galaxies are indicated by open red circles. The error bars correspond to 1σ binomial confidence intervals.

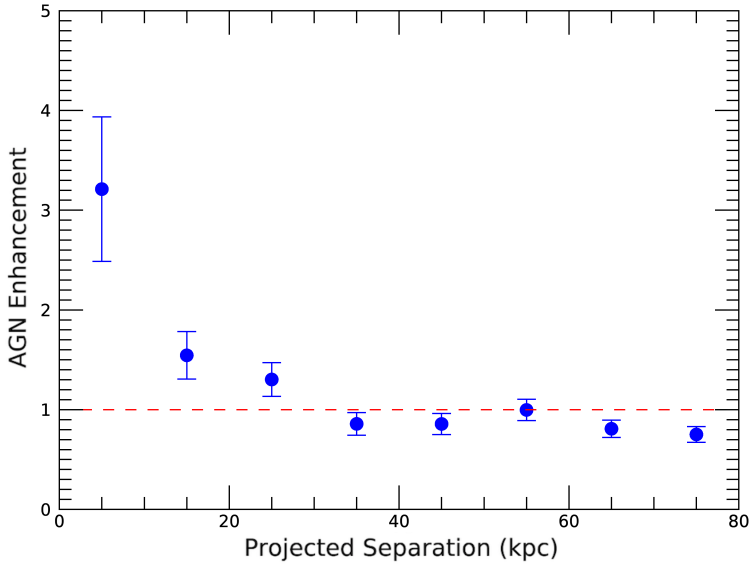

FIG. 5. The level of AGN enhancement as a function of pair separation for all merging galaxies at $0.5 < z < 3.0$ in GDS and EGS. The error bars correspond to appropriate propagation of 1 binomial confidence intervals. The dashed red line reflects an AGN enhancement of 1, where the weighted AGN fractions for control galaxies would exactly equal that for isolated galaxies.

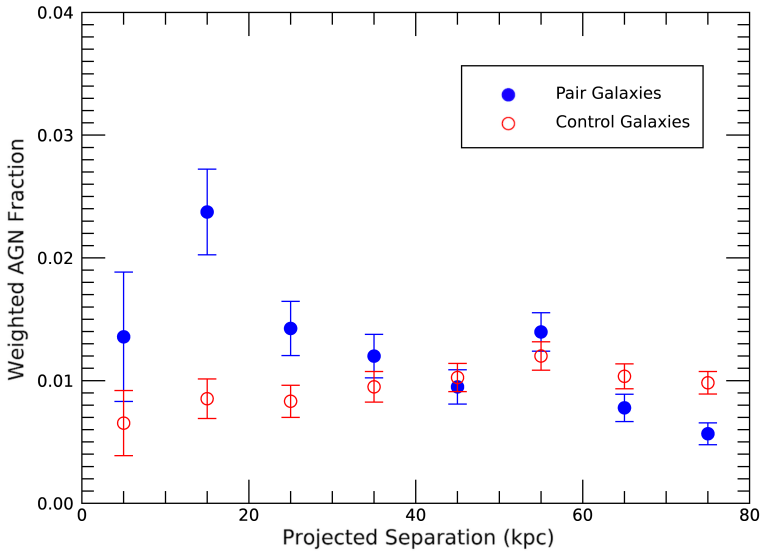

FIG. 6. Weighted AGN fraction as a function of pair separation for galaxies undergoing a minor merger at $0.5 < z < 3.0$ in GDS and EGS. Galaxies with a projected pair are indicated by blue filled circles. Mass- and redshift-matched isolated galaxies are indicated by open red circles. The error bars correspond to 1σ binomial confidence intervals.

of projected separation for all merging galaxies of redshift $0.5 < z < 1.5$ in EGS and GDS is shown in Figure 8, and AGN enhancement as a function of pair separation is shown in Figure 9. Similarly to Figure 5 (figure of all mergers and all redshifts), this sample exhibits increasing AGN enhancements at decreasing projected separations. Galaxies separated by $20 < d < 30$, $10 < d < 20$, and $d < 10$ kpc have AGN enhancements of 1.30 ± 0.28, 1.42 ± 0.33, and 2.38 ± 0.71 respectively.

Weighted AGN fraction as a function of pair separation for all merging galaxies of redshift $1.5 < z < 3.0$ in EGS and GDS is shown in Figure 10. Consequent AGN enhancement as a function of projected separation is shown in Figure 11. In contrast to galaxies at lower redshifts, galaxies of redshift $1.5 < z < 3.0$ do not show any significant AGN enhancement at any projected separation. Galaxies within this sample separated by $20 < d < 30$, $10 < d < 20$, and $d < 10$ kpc have AGN enhancements of 0.68 ± 0.18, 0.89 ± 0.28, and 0.95 ± 0.40 respectively.

In summary, there is a clear trend of increasing AGN enhancement at decreasing pair separations for our entire sample. Major mergers, minor mergers, and low-redshift galaxies all follow this trend. High-redshift galaxies with a close companion, however, do not exhibit

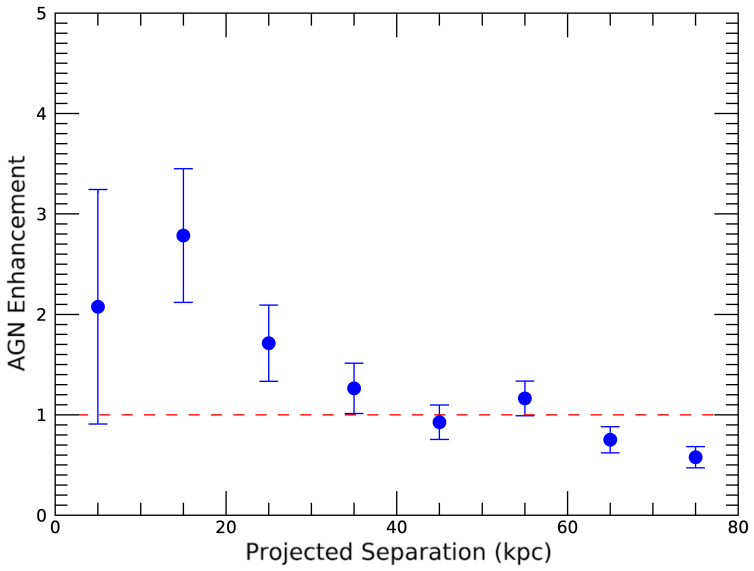

FIG. 7. The level of AGN enhancement as a function of pair separation for galaxies undergoing a minor merger at $0.5 < z < 3.0$ in GDS and EGS. The error bars correspond to appropriate propagation of 1 binomial confidence intervals. The dashed red line reflects an AGN enhancement of 1, where the weighted AGN fractions for control galaxies would exactly equal that for isolated galaxies.

significant AGN enhancement.

5. DISCUSSION

Using a sample of all interacting galaxies of redshift $0.5 < z < 3.0$, we find clear evidence of AGN enhancement at low projected separations. In this section, we discuss the implications of our results in terms of the role mergers play in triggering AGN as well as how galaxy properties alter that role. Additionally, we discuss some caveats and limitations that could be improved upon by later works to increase the significance of our results.

5.1 The AGN-Merger Connection

Based on the results from Figure 5, we see distinct evidence that AGN enhancement increases with decreasing projected separations beginning at 30 kpc. Our results show that merging galaxies separated by more than 30 kpc show no significant AGN enhancement

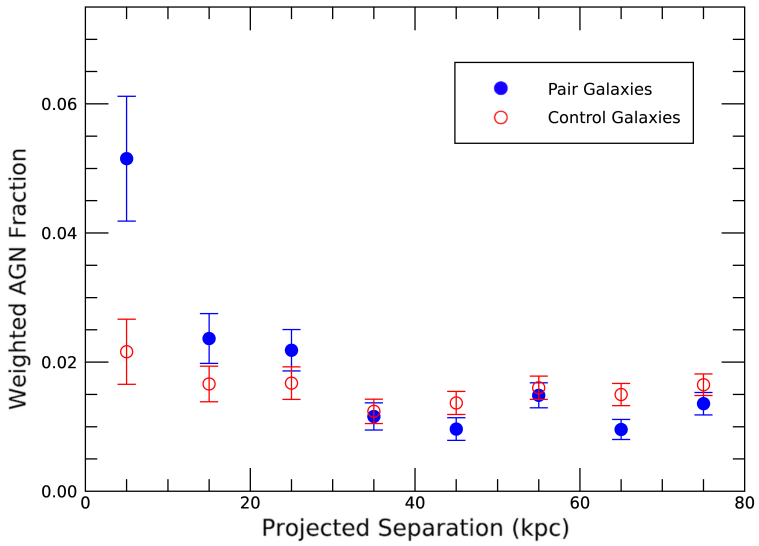

FIG. 8. Weighted AGN fraction as a function of pair separation for all merging galaxies at $0.5 < z < 1.5$ in GDS and EGS. Galaxies with a projected pair are indicated by blue filled circles. Mass- and redshift-matched isolated galaxies are indicated by open red circles. The error bars correspond to 1σ binomial confidence intervals.

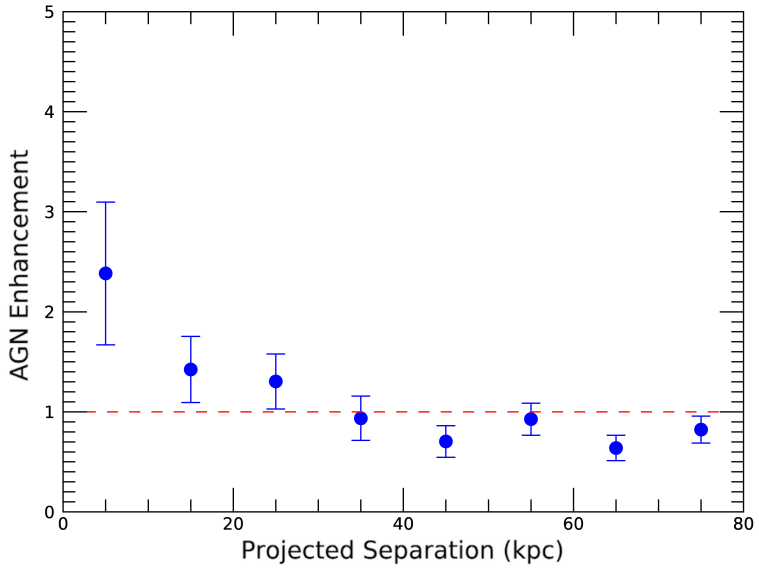

FIG. 9. The level of AGN enhancement as a function of pair separation for all merging galaxies at $0.5 < z < 1.5$ in GDS and EGS. The error bars correspond to appropriate propagation of 1 binomial confidence intervals. The dashed red line reflects an AGN enhancement of 1, where the weighted AGN fractions for control galaxies would exactly equal that for isolated galaxies.

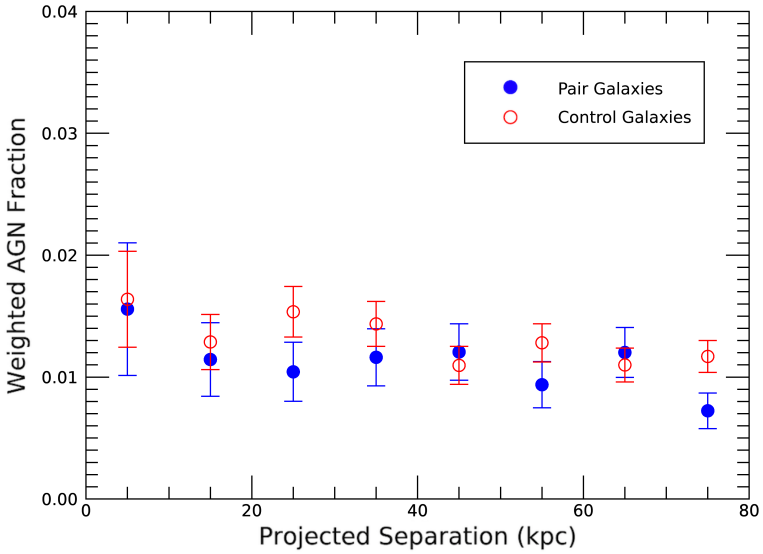

FIG. 10. Weighted AGN fraction as a function of pair separation for all merging galaxies at $1.5 < z < 3.0$ in GDS and EGS. Galaxies with a projected pair are indicated by blue filled circles. Mass- and redshift-matched isolated galaxies are indicated by open red circles. The error bars correspond to 1σ binomial confidence intervals.

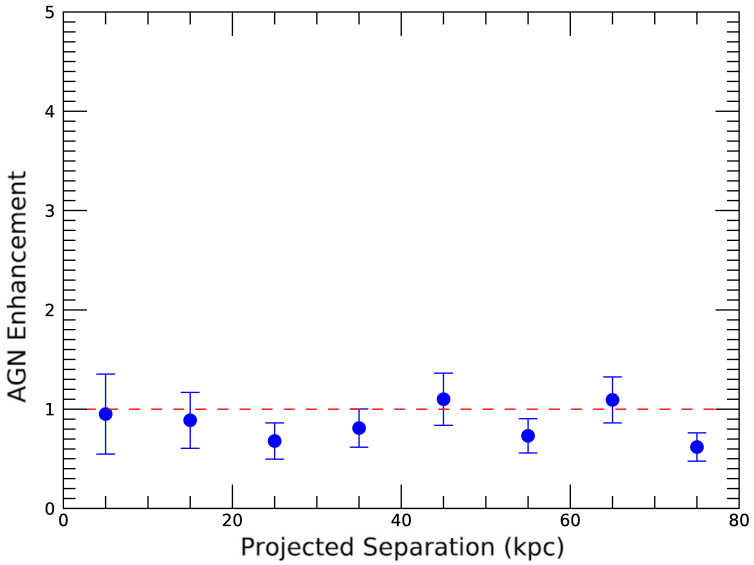

FIG. 11. The level of AGN enhancement as a function of pair separation for all merging galaxies at $1.5 < z < 3.0$ in GDS and EGS. The error bars correspond to appropriate propagation of 1 binomial confidence intervals. The dashed red line reflects an AGN enhancement of 1, where the weighted AGN fractions for control galaxies would exactly equal that for isolated galaxies.

when compared to samples of isolated galaxies. The slightly exponential increase in AGN enhancement suggests a couple of consequences merging galaxies have on growing SMBHs. First, the fact that AGN are detected less frequently at projected separations $20 < d < 30$ than at $d < 10$ implies that there might be a delay between when AGN are triggered when they are detectable. Second, the sharp increase in AGN enhancement at the two lowest separation bins suggests that SMBHs might grow faster as merging galaxies move closer together. By extension, this implies that gas inflow rates into the central SMBH also increases with decreasing pair separation.

We compare the results from Figure 5 to those of similar studies in Figure 12. Our results are in agreement with those of Ellison et al. (2013a), who use optically identified AGN in SDSS. They find a gradual increase in AGN enhancement for pairs of decreasing projected separation beginning at 40 kpc in a sample of major mergers at $0.01 < z < 0.20$. Somewhat surprisingly, however, our results are in stark contrast to Shah et al. (2020), which finds no enhancement of X-ray selected AGN for pairs at any projected separation in a sample of major mergers at $0.5 < z < 3.0$ in the COSMOS and CANDELS surveys. There are a few important distinctions between our study and theirs that could explain the conflicting results.

In comparison to the majority of studies that investigate the effects of galaxy interactions on AGN enhancement, Shah et al. (2020) present a large sample of interacting galaxies at high redshifts. While they find no significant AGN enhancement in galaxies of either $0.5 < z < 1.0$ or $1.0 < z < 3.0$, their findings, in conjunction with much of literature of this field, suggest that galaxy interactions are not primary triggers of AGN activity in high-redshift galaxies (beginning at $z \sim 0.5$). While Figure 5 is in direct contrast to their findings on galaxies at $0.5 < z < 3.0$, Figure 11 supports this high-redshift narrative. Since higher-redshift galaxies have higher gas fractions, they might not require outside catastrophic events, such as a merger, to trigger inflows into the SMBH. In highly gaseous systems, hydrodynamic instabilities could result in gas clumping together, losing angular momentum, and falling into the SMBH. Additionally, the clumpy gas distribution of these galaxies might inhibit gas inflows in the event of a galaxy interaction. Inversely, the lack of AGN enhancement observed at high redshifts could be the product of incomplete merger or AGN surveys. Considering galaxies at high redshifts appear fainter and smaller compared to those in the nearby universe, accurately identifying their mergers or AGN is

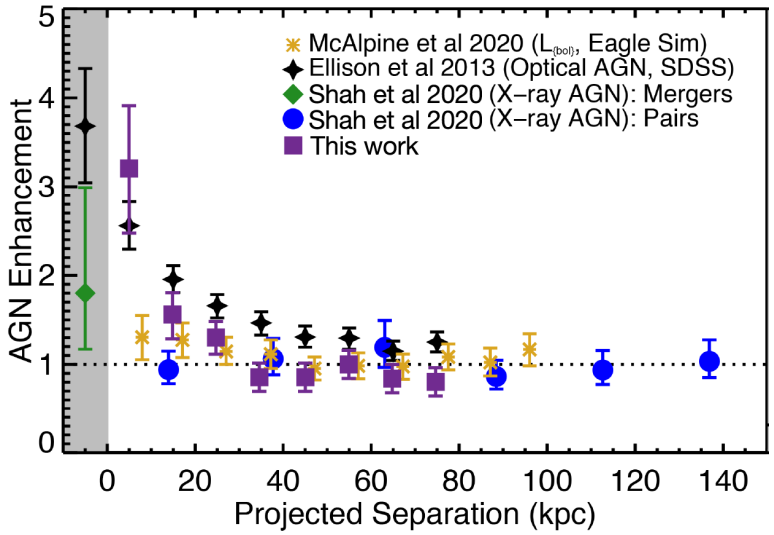

FIG. 12. Modified from Shah et al. (2020), a comparison of our results to similar studies of AGN enhancement as a function of projected separation. Results of Figure 5 (purple squares) plotted with those of Ellison et al. (2013a), who use optical AGN and spectroscopic major mergers in SDSS (black diamonds), McAlpine et al. (2020), who use AGN of $L_{\rm bol} > 10^{42}$ erg s^{-1} and major mergers at $0.05 < z < 0.10$ in the EAGLE cosmological simulation (golden asterisks), and Shah et al. (2020), who use X-Ray AGN and spectroscopic major mergers at $0.5 < z < 3.0$ in COSMOS and CANDELS (blue circles). The gray region corresponds to post-merger systems.

especially challenging. Moreover, observational studies suggest that high-redshift AGN are highly obscured, which further complicates any attempt to observe them. Still, our method of using photometric redshift PDFs and a probabilistic pair count methodology uniquely positions our study to account for some of the uncertainties associated with properties of galaxies at high redshifts. This is especially relevant when compared to Shah et al. (2020), which uses only spectroscopic redshifts in their analysis. The fact that our median redshift is substantially higher than theirs (~ 1.5 vs ~ 1.0) is proof that our study better surveys galaxies at high-redshifts.

In order to survey a variety of galaxies at this stage in our research, we elected to include EGS, a relatively wide field, and GDS, a relatively deep field. This means that the X-ray data, and the AGN survey by extension, is more complete at higher redshifts in GDS than it is in EGS. AGN enhancement as a function of pair separation for all merging galaxies at $1.5 < z < 3.0$ in GDS is shown in Figure 13. Beginning at 20 kpc, there is a slight increase

in AGN enhancement as pair separation decreases. The AGN enhancements for galaxies separated by $10 < d < 20$ and $d < 10$ kpc are 1.50 ± 0.61 and 1.78 ± 1.15 respectively. While the errors are substantial, these results indicate that more accurate data could reveal that AGN activity is indeed enhanced by galaxy interactions at high redshifts.

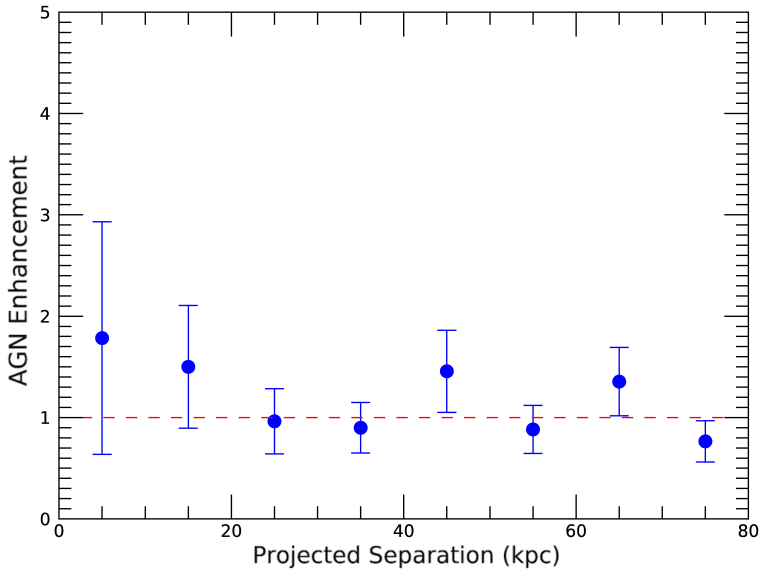

FIG. 13. The level of AGN enhancement as a function of pair separation for all merging galaxies at $1.5 < z < 3.0$ in GDS. The error bars correspond to appropriate propagation of 1 binomial confidence intervals. The dashed red line reflects an AGN enhancement of 1, where the weighted AGN fractions for control galaxies would exactly equal that for isolated galaxies.

Aside from different levels of survey completeness between studies, the discrepancy in enhancements could be due to merger mass ratio selections. Shah et al. (2020) includes only major mergers while our study incorporates both major and minor mergers. As previously referenced, in a survey of interacting galaxies in the nearby universe ($0.01 < z < 0.20$), Ellison et al. (2011) find that AGN enhancement is only mildly correlated with merger mass ratios such that the highest enhancements exist within the sample of major mergers. Conversely, our findings, Figure 7 in particular, indicate that minor mergers play a more important role in triggering AGN than many studies previously suggest. Some simulations show that AGN enhancement actually peaks in minor mergers. Our study is one of the first to thoroughly examine high-redshift minor mergers in the context of AGN enhancement, and, in the future, we hope to investigate further how the impact of minor mergers on AGN activity changes with redshift. Still, our findings in conjunction with the fact that minor

mergers make up the majority of merging galaxies imply that Shah et al. (2020) should see some AGN enhancement if they include minor mergers in their sample. However, as spectroscopic redshifts are more widely available for more massive galaxies, proper inclusion of minor mergers with satellite galaxies in their methodology may be insufficient. Even in our analysis, most minor mergers are missed due their relative faintness and consequently high photometric redshift uncertainty. This is why only $\sim 30\%$ of all included mergers are minor mergers despite their known majority. Considering they observe some AGN enhancement in merging/post-merger systems, it is likely that including true minor mergers at $0.5 < z < 3.0$ could reveal a trend of increasing AGN enhancement at decreasing separations climaxing during post-merger phases.

Moreover, our control sample selection varies considerably from that of Shah et al. (2020). Where we assemble a mass- and redshift- matched control sample with no projected pair within 80 kpc, Shah et al. (2020) Assemble a mass-, redshift- (spectroscopic only), and environment-matched control sample with no projected pair within a Δz corresponding to a relative velocity less than 5000 km s^{-1} out to 150 kpc. The first issue with their control sample has to do with redshift selection. Since their analysis relies only on galaxies with spectroscopic redshifts, they are limited in their isolated galaxy selection. In other words, in order to know whether a projected pair has a relative velocity greater than 5000 km s^{-1}, they need a redshift estimate with low uncertainty for each galaxy in that projected pair. Likewise, it is possible that many isolated galaxies in their control sample may actually have partner satellite galaxies that they cannot properly resolve. A control sample of spectroscopic galaxies may also be biased towards more massive and luminous galaxies, which are more likely to host an AGN. Their second issue has to do with controlling overdensities. By environmentally matching control galaxies to pair galaxies, they may actually be matching conditions they should be isolating. Comparing AGN activity in merging galaxies to that in isolated galaxies directly involves comparing two entirely different environments, one that is merging and one that is not. This discrepancy could result in a bias in their control sample towards overdense environments.

5.2 Caveat and Future Work

While our results have clear implications, it is worth noting some limitations of our method as well as how our study could be improved upon as a whole. One caveat relates to our ability to account for systems of more than two interacting galaxies at similar projected separations. As previously mentioned, if a prime galaxy has more than one partner galaxy at roughly the same projected separation (falls within the same projected separation bin), then that galaxy will receive the highest pair probability of all its partners. In other words, we have not yet devised a method to appropriately incorporate multiple pair probabilities for one galaxy. Additionally, the same prime galaxy may be sorted into multiple projected separation bins based on how far away it is to its partner galaxies. Those prime galaxies will receive different pair probabilities. As a result, it is possible, for example, that an AGN would be weighted as 0.90 (pair probability) by a pair 67 kpc away and as 0.09 by a pair 12 kpc away; the same AGN would be weighted differently in different projected separation bins. While using pair probabilities as AGN weights accounts for most line-of-sight projected pairs, our study does not distinguish or isolate which partner galaxy in a merging system is most responsible for triggering an AGN.

Another limitation of our study has to do with data completeness. While a major strength of our methodology is its ability to incorporate large samples of merging galaxies with photometric redshifts, we are still limited by our ability to resolve particularly small, faint, or obscured galaxies. Within the limitations of our available data and modern detection techniques, there are a couple of additional steps we could take to improve the significance of our results. First, we could simply include the other fields of the CANDELS survey (GDN, UDS, and COSMOS). Although these fields cover varying levels of optical and X-ray depth, incorporating them would increase our merger and AGN sample size, which would improve the statistical significance of our findings. Second, we could add AGN detected using IR broadband colors into our study, as highly obscured galaxies can potentially block X-ray emission from an AGN. We would have to do this carefully, however, as IR surveys of AGN could be biased towards galaxies with intense star forming regions.

Finally, new observing facilities should hopefully give us more complete data at higher redshifts, particularly in the redshift range we are focused on. Some of these facilities that are set to open this decade include the *James Webb Space Telescope* (JWST), the Vera

Rubin Observatory, Euclid, and the *Nancy Grace Roman Space Telescope*. Surveys taken by these facilities would improve identification of both mergers, in clearer morphological signs of disturbances, and AGN, in deeper X-ray and IR data. This would also give us an opportunity to properly identify both merging galaxies with $d < 5$ kpc and post-merger systems, which requires sufficient visual classification.

6. SUMMARY

We used photometric redshift probability distribution functions and a probabilistic pair count methodology to identify a large sample of merging galaxies at $0.5 < z < 3.0$ in EGS and GDS. Using pair statistics, we then counted fractional AGN in order to determine weighted AGN fractions for pairs at different projected separations while accounting for the uncertainties in photometric redshift estimates. We constructed a stellar mass- and redshift-matched control sample of isolated galaxies with no partner within 80 kpc. We assigned each control galaxy the average pair probability of their respective fields, and we used their weighted AGN fraction to calculate AGN enhancement, which we define as the ratio of the weighted AGN fraction for merging galaxies to that of isolated galaxies. We also investigate the effects of selecting samples of different merger mass ratios and redshifts. Based on our determined AGN enhancements, we find:

1. **Galaxy interactions can trigger AGN.** In our broadest sample, we find slight AGN enhancement for galaxies with a pair within 10 to 30 kpc (1.30 ± 0.17 with $20 < d < 30$ kpc and 1.54 ± 0.24 with $10 < d < 20$) and significant enhancement for galaxies that have a pair within 10 kpc (3.21 ± 0.72). The gradual increase in enhancement at decreasing projected separations suggests that either there is a delay between when a merger triggers an AGN and when that AGN is detectable or the rate of SMBH growth increases as merging galaxies move closer together.

2. **Minor mergers play a crucial role in triggering AGN at high redshifts.** We find AGN enhancement in galaxies undergoing a minor merger out to 40 kpc. Enhancement peaks at 2.78 ± 0.66 for galaxies separated by $10 < d < 20$ kpc. We attribute the decrease of enhancement in merging galaxies separated by $d < 10$ kpc to difficulties associated with distinguishing two galaxies of substantially different mass

and luminosity at such small separations.

3. **AGN enhancement decreases with increasing redshift.** While our sample of merging galaxies at $0.5 < z < 1.5$ exhibit increasing AGN enhancements at decreasing pair separations peaking at 2.38 ± 0.71 with $d < 10$ kpc, the sample at $1.5 < z < 3.0$ shows no evidence of enhancement whatsoever. This result suggests that the properties of high-redshift galaxies, such as high gas fractions and clumpy gas distributions, either inhibit gas inflows or promote AGN triggered by secular processes. This outcome could also be the product of incomplete X-ray surveys within this redshift range, as the sample from just GDS, which has deeper X-ray data than EGS, reveals potential enhancement at low separations albeit with relatively high errors.

7. REFERENCES

Akylas, A., Georgakakis, A., Georgantopoulos, I., Brightman, M., Nandra, K. 2012, AA, 546, A98

Alexander, D. M., Smail, I., Bauer, F. E., et al. 2005, Natur, 434, 738

Alonso M. S., Tissera P. B., Coldwell G., Lambas D. G., 2004, MNRAS, 352, 1081

Alonso, M. S., Lambas, D. G., Tissera, P., Coldwell, G. 2007, MNRAS, 375, 1017

Arnouts, S., Ilbert, O. 2011, LePHARE: Photometric Analysis for Redshift Estimate, Astrophysics Source Code Library, ascl:1108.009

Barnes, J. E., Hernquist, L. E. 1991, ApJL, 370, L65

Barro, G., Faber, S. M., Koo, D. C., et al. 2017, ApJ, 840, 47

Barton E. J., Geller M. J., Kenyon S. J., 2000, ApJ, 530, 660

Bell, E. F., Phleps, S., Somerville, R. S., et al. 2006, ApJ, 652, 270

Bluck, A. F. L., Conselice, C. J., Bouwens, R. J., et al. 2009, MNRAS: Letters, 394, L51

Bolzonella, M., Miralles, J.-M., Pell´o, R. 2000, AA, 363, 476

Brammer, G. B., van Dokkum, P. G., Coppi, P. 2008, ApJ, 686, 1503

Bundy, K., Fukugita, M., Ellis, R. S., et al. 2009, ApJ, 697, 1369

Calzetti, D., Armus, L., Bohlin, R. C., et al. 2000, ApJ, 533, 682

Cameron, E. 2011, PASA, 28, 128

Chabrier, G. 2003, ApJL, 586, L133

Cirasuolo, M., McLure, R. J., Dunlop, J. S., et al. 2007, MNRAS, 380, 585

Cisternas, M., Jahnke, K., Inskip, K. J., et al. 2011, ApJ, 726, 57

Civano, F., Elvis, M., Brusa, M., et al. 2012, ApJS, 201, 30

Comastri, A., Setti, G., Zamorani, G., Hasinger, G. 1995, AA, 296, 1

Daddi, E., Alexander, D. M., Dickinson, M., et al. 2007, ApJ, 670, 173

Daddi, E., Elbaz, D., Walter, F., et al. 2010, ApJL, 714, L118

Dahlen, T., Mobasher, B., Faber, S. M., et al. 2013, ApJ, 775, 93

Kodra, D., 2019, Doctoral Dissertation, University of Pittsburgh (Unpublished)

Darg, D. W., Kaviraj, S., Lintott, C. J., et al. 2010, MNRAS, 401, 1552

Davis, M., Guhathakurta, P., Konidaris, N. P., et al. 2007, ApJL, 660, L1

Di Matteo, P., Bournaud, F., Martig, M., et al. 2008, AA, 492, 31

Di Matteo, T., Springel, V., Hernquist, L. 2005, Natur, 433, 604

Donley, J. L., Kartaltepe, J., Kocevski, D., et al. 2018, ApJ, 853, 63

Donley, J. L., Rieke, G. H., Pérez-González, P. G., Rigby, J. R., Alonso-Herrero, A. 2007, ApJ, 660, 167

Draper, A. R., Ballantyne, D. R. 2012, ApJ, 751, 72

Duncan, K. J., Conselice, C. J., Mortlock, A., et al. 2014, MNRAS, 444, 2960

Duncan, K. J., Conselice, C. J., Mundy, C., et al. 2019, ApJ, 876, 110

Ellison, S. L., Mendel, J. T., Patton, D. R., Scudder, J. M. 2013a, MNRAS, 435, 3627

Ellison, S. L., Mendel, J. T., Scudder, J. M., Patton, D. R., Palmer, M. J. D. 2013b, MNRAS, 430, 3128

Ellison, S. L., Patton, D. R., Mendel, J. T., Scudder, J. M. 2011, MNRAS, 418, 2043

Ellison, S. L., Patton, D. R., Simard, L., McConnachie, A. W. 2008, AJ, 135, 1877

Ellison, S. L., Patton, D. R., Simard, L., et al. 2010, MNRAS, 407, 1514

Ellison, S. L., Viswanathan, A., Patton, D. R., et al. 2019, MNRAS, 487, 2491

Fensch, J., Renaud, F., Bournaud, F., et al. 2017, MNRAS, 465, 1934

Fontana, A., D'Odorico, S., Poli, F., et al. 2000, AJ, 120, 2206

Galametz, A., Grazian, A., Fontana, A., et al. 2013, ApJS, 206, 10

Gebhardt, K., Bender, R., Bower, G., et al. 2000, ApJL, 539, L13

Giallongo, E., D'Odorico, S., Fontana, A., et al. 1998, AJ, 115, 2169

Giavalisco, M., Ferguson, H. C., Koekemoer, A. M., et al. 2004, ApJL, 600, L93

Gilli, R., Comastri, A., Hasinger, G. 2007, AA, 463, 79

Grogin, N. A., Conselice, C. J., Chatzichristou, E., et al. 2005, ApJL, 627, L97

Grogin, N. A., Kocevski, D. D., Faber, S. M., et al. 2011, ApJS, 197, 35

Gültekin, K., Richstone, D. O., Gebhardt, K., et al. 2009, ApJ, 698, 198

Guo, Y., Ferguson, H. C., Giavalisco, M., et al. 2013, ApJS, 207, 24

Hopkins P. F., 2011, MNRAS, 420, L8

Hopkins P. F., Hernquist L., Hayward C. C., Narayanan D., 2012, MNRAS, 425, 1121

Hopkins P. F., Quataert E., 2010, MNRAS, 407, 1529

Hopkins, P. F., Cox, T. J., Younger, J. D., Hernquist, L. 2009, ApJ, 691, 1168

Hsu, L.-T., Salvato, M., Nandra, K., et al. 2014, ApJ, 796, 60

Ilbert, O., McCracken, H. J., Le Fèvre, O., et al. 2013, AA, 556, A55

Johansson, P. H., Burkert, A., Naab, T. 2009, ApJL, 707, L184

Kartaltepe, J. S., Sanders, D. B., Scoville, N. Z., et al. 2007, ApJS, 172, 320

Kennicutt R. C., Jr, Roettiger K. A., Keel W. C., van der Hulst J. M., Hummel E., 1987, AJ, 93, 1011

Kewley L. J., Geller M. J., Barton E. J., 2006a, AJ, 131, 2004

Kewley L. J., Rupke D., Jabran Z. H., Geller M. J., Barton E. J., 2010, ApJ, 721, L48

Kitzbichler M. G., White S. D. M., 2008, MNRAS, 391, 1489

Kocevski, D. D., Barro, G., Faber, S. M., et al. 2017, ApF, 846, 112

Kocevski, D. D., Brightman, M., Nandra, K., et al. 2015, ApJ, 814, 104

Kocevski, D. D., Faber, S. M., Mozena, M., et al. 2012, ApJ, 744, 148

Koekemoer, A. M., Faber, S. M., Ferguson, H. C., et al. 2011, ApJS, 197, 36

Kriek, M., van Dokkum, P. G., Labbé, I., et al. 2009, ApJ, 700, 221

Lacy, M., Storrie-Lombardi, L. J., Sajina, A., et al. 2004, ApJS, 154, 166

Lambas D. G., Tissera P. B., Alonso M. S., Coldwell G., 2003, MNRAS, 346, 1189

Lawrence, A., Warren, S. J., Almaini, O., et al. 2007, MNRAS, 379, 1599

Le Fèvre, O., Abraham, R., Lilly, S. J., et al. 2000, MNRAS, 311, 565

Li C., Kauffmann G., Heckman T. M., White S. D. M., Jing Y. P., 2008, MNRAS, 385, 1915

López-Sanjuan, C., Cenarro, A. J., Varela, J., et al. 2015, AA, 576, A53

Lotz, J. M., Jonsson, P., Cox, T. J., Primack, J. R. 2008, MNRAS, 391, 1137

Magorrian, J., Tremaine, S., Richstone, D., et al. 1998, AJ, 115, 2285

Man, A. W. S., Toft, S., Zirm, A. W., Wuyts, S., van der Wel, A. 2011, ApJ, 744, 85

McAlpine, S., Harrison, C. M., Rosario, D. J., et al. 2020, MNRAS, 494, 5713

McConnell, N. J., Ma, C.-P. 2013, ApJ, 764, 184

Mendez A. J., Coil A. L., Lotz J., Salim S., Moustakas J., Simard L., 2011, ApJ, 736, 110

Michel-Dansac L., Lambas D. G., Alonso M. S., Tissera P., 2008, MNRAS, 386, 82

Mihos, J. C., Hernquist, L. 1996, ApJ, 464, 641

Mobasher, B., Dahlen, T., Ferguson, H. C., et al. 2015, ApJ, 808, 101

Molino, A., Benitez, N., Moles, M., et al. 2014, MNRAS, 441, 2891

Mortlock, A., Conselice, C. J., Hartley, W. G., et al. 2014, MNRAS, 447, 2

Muzzin, A., Marchesini, D., Stefanon, M., et al. 2013, ApJ, 777, 18

Nandra, K., Laird, E. S., Aird, J. A., et al. 2015, ApJS, 220, 10

Nikolic B., Cullen H., Alexander P., 2004, MNRAS, 355, 874

Patton D. R., Ellison S. L., Simard L., McConnachie A. W., Mendel J. T., 2011, MNRAS, 412, 591

Patton, D. R., Torrey, P., Ellison, S. L., Mendel, J. T., Scudder, J. M. 2013, MNRAS, 433, L59

Peng, C. Y., Ho, L. C., Impey, C. D., Rix, H.-W. 2002, AJ, 124, 266

Pierce, C. M., Lotz, J. M., Laird, E. S., et al. 2007, ApJL, 660, L19

Puech M., Hammer F., Hopkins P. F., et al. 2012, ApJ, 753, 128

Robaina, A. R., Bell, E. F., van der Wel, A., et al. 2010, ApJ, 719, 844

Rupke D. S. N., Kewley L. J., Chien L.-H., 2010, 723, 1255

Santini, P., Ferguson, H. C., Fontana, A., et al. 2015, ApJ, 801, 97

Satyapal, S., Ellison, S. L., McAlpine, W., et al. 2014, MNRAS, 441, 1297

Schawinski K., Virani S., Simmons B., et al. 2009, ApJ, 692, L19

Schawinski, K., Simmons, B. D., Urry, C. M., Treister, E., Glikman, E. 2012, MNRAS, 425, L61

Schawinski, K., Treister, E., Urry, C. M., et al. 2011, ApJL, 727, L31

Scoville, N., Aussel, H., Sheth, K., et al. 2014, ApJ, 783, 84

Scudder, J. M., Ellison, S. L., Torrey, P., Patton, D. R., Mendel, J. T. 2012, MNRAS, 426, 549

Shah, E. A., Kartaltepe, J. S., Magagnoli, C. T., et al. 2020, ApJ, 904, 107

Snyder G. F., Cox T. J., Hayward C. C., Hernquist L., Jonsson P., 2011, ApJ, 741, 77

Snyder G. F., Hayward C. C., Sajina A., et al. 2013, ApJ, 768, 168

Soifer, B. T., Helou, G., Werner, M. 2008, ARAA, 46, 201

Stefanon, M., Yan, H., Mobasher, B., et al. 2017, ApJS, 229, 32

Stern, D., Eisenhardt, P., Gorjian, V., et al. 2005, ApJ, 631, 163

Storchi-Bergmann T., Gonzalez-Delgado R. M., Schmitt H. R., CidFernandes R., Heckman T., 2001, ApJ, 559, 147

Stott, J. P., Swinbank, A. M., Johnson, H. L., et al. 2016, MNRAS, 457, 1888

Sutherland, W., Saunders, W. 1992, MNRAS, 259, 413

Tacconi, L. J., Genzel, R., Neri, R., et al. 2010, Nature, 463, 781

Treister, E., Schawinski, K., Urry, C. M., Simmons, B. D. 2012, ApJL, 758, L39

Tremaine, S., Gebhardt, K., Bender, R., et al. 2002, ApJ, 574, 740

Ueda, Y., Akiyama, M., Ohta, K., Miyaji, T. 2003, ApJ, 598, 886

van der Wel, A., Franx, M., van Dokkum, P. G., et al. 2014, ApJ, 788, 28

Weston, M. E., McIntosh, D. H., Brodwin, M., et al. 2017, MNRAS, 464, 3882

Wiklind, T., Dickinson, M., Ferguson, H. C., et al. 2008, ApJ, 676, 781

Woods, D. F., Geller, M. J. 2007, AJ, 134, 527

Wuyts, S., Förster Schreiber, N. M., Lutz, D., et al. 2011, ApJ, 738, 106

Xue, Y. Q., Luo, B., Brandt, W. N., et al. 2011, ApJS, 195, 10

Xue, Y. Q., Luo, B., Brandt, W. N., et al. 2016, ApJS, 224, 15

Younger J. D., Hayward C. C., Narayanan D., et al. 2009, MNRAS, 396, L66

APPENDIX I: DETAILED AGN ENHANCEMENT DATA

	$0 < d < 10$	$10 < d < 20$	$20 < d < 30$	$30 < d < 40$	$40 < d < 50$	$50 < d < 60$	$60 < d < 70$	$70 < d < 80$
Paired Galaxies	365	1206	1782	2211	2612	3108	3336	3854
AGN	20	47	80	93	103	138	131	163
Fractional AGN	10.55	15.86	20.36	17.14	19.60	27.21	25.13	26.30
Weighted AGN Fraction (%)	2.89 ± 0.39	1.31 ± 0.14	1.14 ± 0.11	0.78 ± 0.08	0.75 ± 0.07	0.88 ± 0.07	0.75 ± 0.06	0.68 ± 0.06
Control Galaxies	648	1962	2871	3515	4107	4808	5135	5886
AGN	30	86	130	164	186	219	248	277
Fractional AGN	5.83	16.70	25.18	31.78	35.96	42.20	47.84	53.45
Weighted AGN Fraction (%)	0.90 ± 0.16	0.85 ± 0.09	0.88 ± 0.08	0.90 ± 0.07	0.88 ± 0.06	0.88 ± 0.06	0.93 ± 0.06	0.91 ± 0.05
AGN Enhancement	3.21 ± 0.74	1.54 ± 0.24	1.30 ± 0.17	0.86 ± 0.11	0.86 ± 0.11	1.00 ± 0.11	0.81 ± 0.09	0.75 ± 0.08

TABLE I. Weighted AGN Fraction and AGN Enhancment: EGS and GDS (all mergers at $0.5 < z < 3.0$)